RSC Advances

PAPER

View Article Online
View Journal | View Issue

Cite this: *RSC Adv.*, 2017, **7**, 21221

Light conversion material: $LiBaPO_4:Eu^{2+}$, Pr^{3+}, suitable for solar cell

Yan Chen, *[a] Jing Wang,*[b] Mei Zhang[a] and Qingguang Zeng[a]

Received 14th February 2017
Accepted 8th April 2017

DOI: 10.1039/c7ra01834g

rsc.li/rsc-advances

A light conversion material $LiBaPO_4:Eu^{2+}$, Pr^{3+} is successfully developed as a solar spectral converter for Si solar cells. The photoluminescence excitation and emission spectra from 3 K to room temperature, the lifetime and energy transfer mechanism are all systematically investigated. The results show that Eu^{2+} ions absorb and transfer the energy of UV-Vis photons to Pr^{3+} ions, which exhibit an intense near-infrared (NIR) emission between 950–1060 nm, matching well with the maximum spectral response of Si solar cells. We believe that this NIR emitting phosphor may open a new route to design advanced UV-Vis-to-NIR phosphors, with promising applications for solar spectral convertors.

1. Introduction

Phosphors doped with rare earth ions (Re^{n+}) are used for many devices such as white light emitting diodes (WLED), displays and so on.[1–3] Recently, they have also attracted much interest for photovoltaic applications to improve solar cell efficiency by modifying the solar spectrum. Si solar cells effectively convert near infrared (NIR) photons of lower energy close to the semiconductor band gap ($E_g \approx 1.12$ eV, $\lambda \approx 1000$ nm). However, the strongest emission of the solar spectrum is located in the UV-Vis region. The mismatch between the strongest emission in the solar spectrum and the spectral response of Si solar cells, will reduce the photoelectric conversion efficiency of the cell.[4,5]

Recently, light conversion material is used to modify the solar spectrum and enhance the external quantum efficiency of Si solar cell.[6–8] Many researches have been developed phosphors doped by Yb^{3+} ion, Eu^{3+}–Yb^{3+}, Tb^{3+}–Yb^{3+}, Dy^{3+}–Yb^{3+}, Eu^{2+}–Yb^{3+} and so on.[9–15] However, Yb^{3+} usually has no direct absorptions in UV-Vis (300–800 nm) range since it only has a single excited state $^2F_{5/2}$ approximately 10 000 cm^{-1} above the ground state $^2F_{7/2}$. Therefore, Re^{3+} (Eu^{3+}, Tb^{3+}, Dy^{3+} and so on) is selected as a sensitizer in Re^{3+}–Yb^{3+} co-doped phosphor. But this kind of materials usually have low absorption efficiency in UV-Vis light range, due to the forbidden 4f–4f transitions by the parity selection rule.

As we know, Pr^{3+} ion has the ability to absorb visible photons and emits NIR photons, because of its abundant energy levels in UV-Vis-NIR range. For instance, Pr^{3+} ion doped phosphors can be excited at the range of 440–700 nm due to the transitions from $^3H_4$ to $^1D_2$ (~600 nm), ^3P_J ($J = 0, 1, 2$) and $^1I_6$ (440–490 nm), and emit NIR phonons at ~1000 nm ascribed to the $^3P_0 \rightarrow {}^1G_4$ and/or $^1G_4 \rightarrow {}^3H_4$, matching well with the optimal spectral response of Si solar cells.[16–19] To enhance the absorption of Pr^{3+} in ultraviolet region, here we explored a promising light conversion phosphor $LiBaPO_4:Eu^{2+}$, Pr^{3+} for Solar Spectral Convertor. It can exhibit an intense NIR emission of Pr^{3+} ion at about 1000 nm upon excitation with allowed 4f–5d absorption of Eu^{2+} ions.

2. Experiment

2.1 Syntheses

All phosphors were prepared by a conventional solid-state method. The stoichiometric amounts of LiH_2PO_4 (97%), $BaCO_3$ (A.R.), $NH_4H_2PO_4$ (A.R.), Eu_2O_3 (99.99%) and Pr_6O_{11} (99.99%) were used as raw materials. Then the ingredients were thoroughly grinded in an agate mortar and transferred into crucibles. Finally, the mixtures were sintered at 1200 °C for 3 h under N_2/H_2 (10 : 1) atmosphere and grounded homogeneously after cooling.

2.2 Measurements

The phase purity of the as-prepared phosphors was investigated by a Rigaku D/max-IIIA X-ray Diffractometer with Cu Kα radiation ($\lambda = 1.5406$ Å) at 40 kV and 30 mA. The XRD patterns were collected in range of $15° \leq 2\theta \leq 58°$.

The photoluminescence (PL) and photoluminescence excitation (PLE) spectra from 3 K to room temperature as well as the decay curves were measured by FSP920 Time Resolved and Steady State Fluorescence Spectrometers (Edinburgh Instruments) equipped with a 450 WW Xe lamp, a 100 W μF920H lamp, TM300 excitation monochromator and double TM300 emission monochromators, red sensitive PMT and R5509-72 NIR-PMT in a liquid nitrogen cooled housing (Hamamatsu Photonics K.K). The spectral resolution for the steady

[a]School of Applied Physics and Materials, Wuyi University, Jiangmen, Guangdong 529020, P. R. China. E-mail: ychen08@163.com; Fax: +86 20 84112112
[b]School of Chemistry, Sun Yat-sen University, Guangzhou, Guangdong 510275, P. R. China. E-mail: ceswj@mail.sysu.edu.cn

measurements is about 0.05 nm in UV-vis and about 0.075–0.01 nm in NIR, and the experimental conditions for the transient measurements are a pulse width of 1–2 μs, a repetition rate of 50 Hz and the lifetime range of 100 μs–200 s. For PL and PLE measurements at 3 K, the sample was mounted in a Optistat AC-V12 actively cooled optical cryostat, based on 0.25 W @ 4 K PTR (pulse tube refrigerator), with a ITC503 temperature controller and a water cooled compressor.

3. Results and discussion

3.1 Phase and structure characterization

The XRD patterns of polycrystalline samples $LiBaPO_4:Eu_x^{2+}$, Pr_y^{3+} ($x = 0, y = 0$; $x = 0.005, y = 0, 0.005$; $x = 0, y = 0.01$) are shown in Fig. 1a. The results indicate that all the peaks of rare earth ions doped $LiBaPO_4$ can be indexed to the Joint Committee On Powder Diffraction Standard card of a pure $LiBaPO_4$ (JCPDS 14-0270), and also match well with the reference data.[20,21] No detectable impurity phases were observed, which indicated that the introduction of dopants has no obvious influence on the crystalline structure of the host, which crystallize in a stuffed tridymite structure with a hexagonal unit cell and space group $P6_3$. Each PO_4 tetrahedron is jointed with four LiO_4 tetrahedron, while each LiO_4 is jointed whit four PO_4 tetrahedrons, and two series of tetrahedron are linked by corner sharing,[21] as shown in Fig. 1b and c. Furthermore, the ionic radius of Eu^{2+}, Pr^{3+}, Ba^{2+} and Li^+ are 1.25 Å, 1.13 Å, 1.42 Å and 0.92 Å, respectively. According to the ionic size and valence state of cationic, Eu^{2+} and Pr^{3+} ions are expected to replace the site of Ba^{2+} ion, since the radius of Eu^{2+} and Tb^{3+} are closed to that of Ba^{2+}.

3.2 Luminescence properties of $LiBaPO_4:Pr^{3+}$

Fig. 2 shows the PL (a and b) and PLE (c) spectra, and decay curves of $LiBaPO_4:Pr_{0.01}^{3+}$ at 3 K. The selection of low test

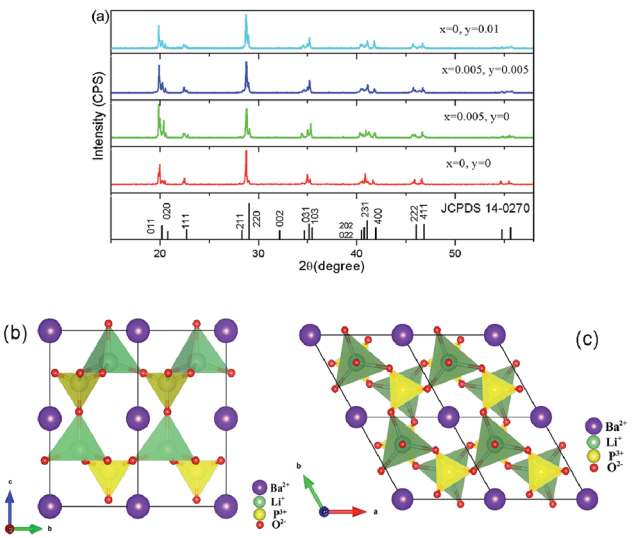

Fig. 1 XRD patterns of $LiBaPO_4:Eu_x^{2+}$, Pr_y^{3+} ($x = 0, y = 0$; $x = 0.005, y = 0, 0.005$; $x = 0, y = 0.01$) (a), and schematic diagram of the structure of $LiBaPO_4$ along the *a*- (b) and *c*-direction (c).

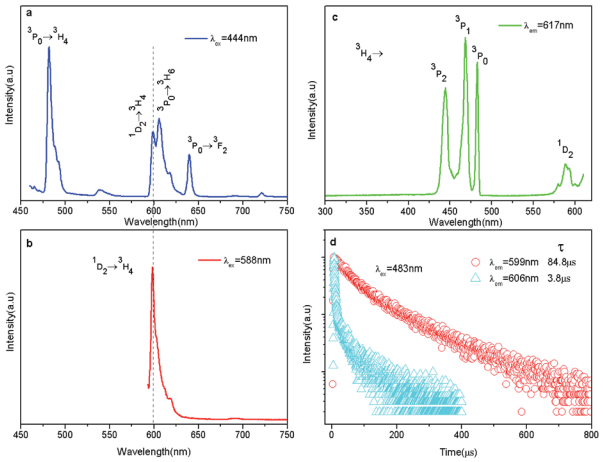

Fig. 2 PL (a and b) and PLE (c) spectrum, and decay curves (d) of $LiBaPO_4:Pr_{0.01}^{3+}$ at 3 K.

temperature is to reduce the effects of the host vibration or phonons on the optical properties of Pr^{3+} ion. As shown in Fig. 2c, the excitation spectrum mainly contains four sharp peaks at 444 nm, 468 nm, 483 nm and 588 nm, which are due to the absorption transitions of $^3H_4 \rightarrow {}^3P_2$, $^3H_4 \rightarrow {}^3P_1$ and $^1I_6$, $^3H_4 \rightarrow {}^3P_0$, and $^3H_4 \rightarrow {}^1D_2$ of Pr^{3+} ion, respectively, monitoring the emission at 617 nm. Fig. 2a and b are the emission spectra of Pr^{3+} ion under excitation from the ground state to the $^3P_2$ and $^1D_2$ levels, respectively. It is obviously that the emission spectrum excited to $^1D_2$ levels (Fig. 2a) consists of only one emission peak at 599 nm, due to the transitions from $^1D_2$ to $^3H_4$. Whereas exited to $^3P_2$ level (Fig. 2b), the emission spectrum consists of not only the emission from $^3P_0$ to $^3H_4$, $^3H_6$ and $^3F_2$ peaked at 482 nm, 606 and 640 nm, but also the emission from $^1D_2$ to $^3H_4$ at 599 nm.

In order to clarify the assignment of the emissions peaks at 599 nm and 606 nm as shown in Fig. 2a, the luminescence decay curves at 3 K (λ_{ex} = 483 nm and 599 nm, λ_{em} = 606 nm) of $LiBaPO_4:Pr_{0.01}^{3+}$ were measured and presented in Fig. 2d. Generally, the decay time of the emission from $^1D_2$ is 50–250 μs, longer than that from $^3P_0$, which is about 0.135–50 μs.[22] It is clear that the decay curves have different characteristics and the average lifetimes are calculated to be about 84.8 μs and 3.8 μs when excited to $^3P_0$ and $^1D_2$ level, respectively. Therefore, it is reasonable to assign the emission peaks at 599 nm and 606 nm to $^1D_2 \rightarrow {}^3H_4$ and $^3P_0 \rightarrow {}^3H_6$ transitions.

However, why can the emission from $^1D_2$ to $^3H_4$ be detected when excited into $^3P_2$ level? The energy transfer through multi-phonon relaxation and cross-relaxation process may give a clear interpretation. Fig. 3 presents the schematic diagrams of Pr^{3+} in $LiBaPO_4$. It is widely accepted that the electrons excited to $^3P_2$ level (2a) are able to relax to $^3P_0$ level assisted by phonons (process 2b), because of the small energy difference between $^3P_2$ and $^3P_0$ level. There are two possible non-radiative path to generate the $^1D_2 \rightarrow {}^3H_4$ transition (process 2c and 2d). One is the non-radiative relaxation from $^3P_0$ to $^1D_2$ level assisted by phonons, which is labeled as process 2c. The energy difference between $^3P_0$ and $^1D_2$ level is about 3697 cm^{-1}. The maximum

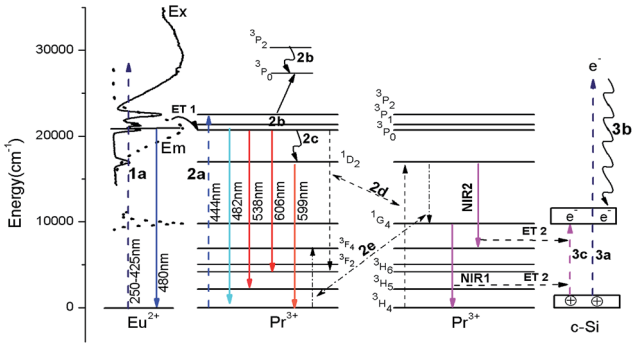

Fig. 3 Schematic diagrams of the cross-relaxation processes and ET from Eu^{2+} to Pr^{3+} in $LiBaPO_4$ and from Pr^{3+} to Si solar cells. (2d: [$^3P_0$, $^3H_4$] → [$^3H_6$, $^1D_2$]; 2e: [$^1D_2$, $^3H_4$] → [$^1G_4$, $^3F_4$]; 3b: the lattice thermalization loss).

vibration frequency of phosphate is about 1037 cm^{-1}.[23] It means that three phonons are required to bridge this energy gap. Generally, phonons assisted non-radiative relaxation process from the upper level to the lower level is possible, if the energy gap is less than 5 times the energy of the highest energy phonon. Therefore, it is expected that multi-phonon relaxation process from $^3P_0$ to $^1D_2$ level may occur in $LiBaPO_4:Pr^{3+}$. The other is cross-relaxation process (2d), [$^3P_0$, $^3H_4$] → [$^3H_6$, $^1D_2$]. The energy gaps between $^3P_0$ and $^3H_6$ level, and $^1D_2$ and $^3H_4$ level are 16 502 cm^{-1} and 17 007 cm^{-1}, respectively. The difference between them is only about 505 cm^{-1}. Therefore, the cross-relaxation [$^3P_0$, $^3H_4$] → [$^3H_6$, $^1D_2$] (2d) is also efficient. In a word, the whole blue-to-red ET process could be expressed as (2a → 2b → 2c/2d → 599 nm) for the red emissions from the $^1D_2$ level and (2a → 2b → 606 nm) from the $^3P_0$ level.

To further study the effect of phonon to luminescence property of Pr^{3+} in $LiBaPO_4$, Fig. 4a presents the normalized emission spectra of $LiBaPO_4:Pr_{0.01}{}^{3+}$ at different temperature. It's interesting to observe the temperature dependence of $^3P_1$ → $^3H_5$ transition peaked at 523 nm when excited into $^3P_0$ level. At 3–100 K, Pr^{3+} ion gives no emission at 523 nm whereas above 100 K the $^3P_1$ → $^3H_5$ transition is clearly observed. Moreover, its emission intensity regularly increases with the increase of temperature. This phenomenon is due to the increase of electron–phonon interaction, which leads to more and more electrons populated from $^3P_0$ up to $^3P_1$ level with the rise of the temperature. In addition, the intensity ratio of $^1D_2$ → $^3H_4$ to $^3P_0$ → $^3H_6$ increases gradually with temperature increases, as shown in Fig. 3b, which strongly proves cross-relaxation or multi-phonon relaxation process (Fig. 3, 2d and c) from $^3P_0$ to $^1D_2$ level is efficient especially at room temperature. However, it is very hard to make a decision which one is dominant between multi-phonon relaxation process (2c) and cross-relaxation process (2d).

The energy difference between transition $^1G_4$ → $^1D_2$ (7203 cm^{-1}) and $^3H_4$ → $^3F_4$ (6854 cm^{-1}), is calculated to be only about 349 cm^{-1}, as shown in Fig. 3. Thus, the cross-relaxation (2e), [$^1D_2$, $^3H_4$] → [$^1G_4$, $^3F_4$] will happen due to the small energy mismatch. In other words, electrons populate to the $^1G_4$ level by two steps of cross-relaxation (2d–2e) when excited into $^3P_0$ level. Consequently, it is theoretically expected that the NIR1 emissions from the $^1G_4$ level could be observed. Fig. 5a presents the emission spectra of $LiBaPO_4:Pr_{0.01}{}^{3+}$ in NIR region at room temperature. Up to $^3P_0$ (483 nm) and $^1D_2$ (590 nm) level, the strong NIR emission at 1020 nm is observed and attributed to the transition of $^1G_4$ → $^3H_4$. The above results further prove that the cross-relaxation (2e), [$^1D_2$, $^3H_4$] → [$^1G_4$, $^3F_4$], is occurred in $LiBaPO_4:Pr_{0.01}{}^{3+}$. Beside the prominent NIR1 emission at 1020 nm, Pr^{3+} ion also gives the NIR2 emissions at 976 nm and 993 nm, attributed to the transitions from different sublevels of $^1D_2$ to $^3F_4$ level. To sum up, the process of NIR emissions from $^1G_4$ and $^1D_2$ levels could be expressed as (2b → 2c/2d → 2e → NIR1 and 2b → 2c/2d → NIR2), as shown in Fig. 3.

For the sake of verifying the assignment of emission at 976 nm, 993 nm and 1020 nm, Fig. 5b shows normalized decay curves and lifetime of $LiBaPO_4:Pr_{0.01}{}^{3+}$ at room temperature. If the emission transitions from the different stark levels of

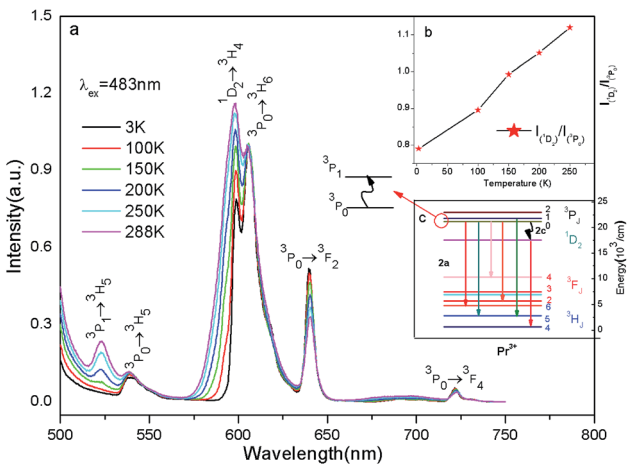

Fig. 4 Normalized emission spectra of $LiBaPO_4:Pr_{0.01}{}^{3+}$ at 3–300 K (a). Inset is the intensity ratio of $^1D_2$ → $^3H_4$ to $^3P_0$ → $^3H_6$ as a function of temperature (b) and the energy diagram of $LiBaPO_4:Pr_{0.01}{}^{3+}$ (c).

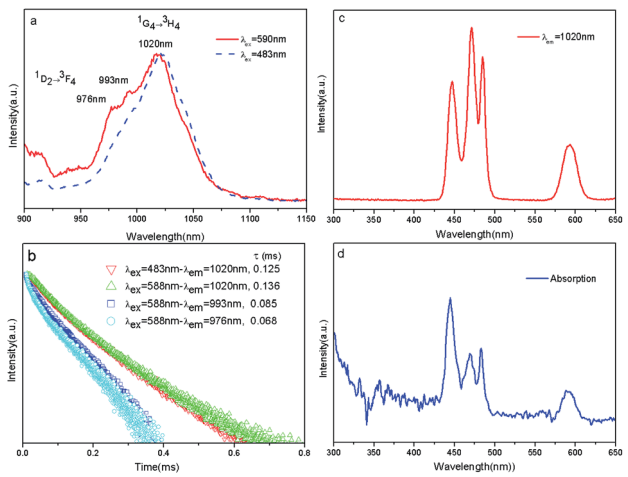

Fig. 5 Normalized PLE (a) and PL spectrum (b), decay curves (c) and absorption spectrum (d) of $LiBaPO_4:Pr_{0.01}{}^{3+}$ at room temperature.

a excited level to a ground level, it is expect to have the approximated lifetime when up to the same excited levels. The lifetimes of emission at 1020 nm are 0.125 ms and 0.136 ms excited to $^3P_0$ level (483 nm) and $^1D_2$ level (588 nm), respectively. Similarly, the lifetimes of emissions at 993 nm and 976 nm are 0.085 ms and 0.068 ms excited to $^1D_2$ level (588 nm). That is to say the emissions at 993 nm and 976 nm belong to the same transition, different to the 1020 nm. It is clearly that the lifetime of emission at 1020 nm is longer than that of the 993 nm and 976 nm because of the two steps of cross-relaxation processes. Therefore, the emissions at 976 nm (or 993 nm) and 1020 nm are attributed to the transitions of $^1D_2 \rightarrow {}^3F_4$ and $^1G_4 \rightarrow {}^3H_4$, respectively.

According to the report of A. Meijerink,[24] the absorption of a photon to the ^3P_J or $^1I_6$ levels would be followed by the emission of two NIR photons, whereas absorption to $^1D_2$ would result in emission of only one NIR photon. If the area ratio (R_E) of the ^3P_J and $^1I_6$ band to $^1D_2$ band in the excitation spectrum is twice as large as the ratio (R_A) similarly obtained in the absorption spectra, the quantum cutting will be efficient. Fig. 5c and d show the excitation spectrum and the absorption spectrum of $LiBaPO_4:Pr_{0.01}^{3+}$. It can be found in Fig. 5c and d that the R_E and R_A are 4.0 and 4.4, respectively. It means that the blue-to-NIR quantum cutting process from the $^3P_0$ level does not occur in $LiBaPO_4$.

As mentioned above, the ideal light conversion material for Si solar cells should utilize the UV-vis region of the solar spectrum and possess an intense NIR emission, matching well with the maximum spectral response ($\lambda \approx 1000$ nm) of Si semiconductor. As shown in Fig. 5a and c, $LiBaPO_4:Pr^{3+}$ meets the requirement of excitation and emission characteristics of light conversion material. However, it can only absorb the photons in blue and red region of the solar spectrum. Unfortunately, the intensity of the excitation peaks is very weak because the 4f–4f absorption transitions are forbidden by the parity selection rule. In order to widen the utilization of the solar spectrum towards UV region, we further investigate the luminescent properties of $LiBaPO_4:Eu^{2+},Pr^{3+}$ and explore the possibility of Eu^{2+} ion as donor absorbing UV photons, which greatly enhances the NIR emission of Pr^{3+} ion through efficient energy feeding by allowed 4f–5d absorption of Eu^{2+} ion with high oscillator strength.

3.3 Luminescence properties of $LiBaPO_4:Eu_{0.005}^{2+}$, $Pr_{0.005}^{3+}$

As discussed above, $LiBaPO_4:Eu_{0.005}^{2+}$, $Pr_{0.005}^{3+}$ phosphor shows the optimal NIR performance. In order to explore its possibility of potential application in Si solar cells, as shown in Fig. 6c. It is obviously seen that Si solar cells most effectively convert photons of energy close to the semiconductor band gap ($E_g \approx$ 1.12 eV, 1000 cm^{-1}), but the incident solar spectrum dominates in UV-Vis region. This mismatch between the incident solar spectrum and the spectral response of Si solar cells is one of the main reasons to limit the efficiency of cell. For instance, a UV photon with high energy (250–425 nm) directly creates an electron–hole (e–h) pair in Si solar cells (Fig. 3a). However, the photo-excited pair quickly loses energy in excess of band gap of Si and the extra energy is lost as heat within the device (Fig. 3b).

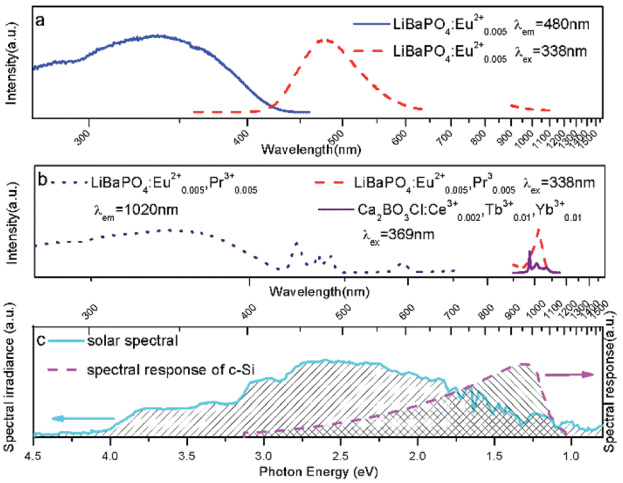

Fig. 6 PLE and PL spectra of $LiBaPO_4:Eu_{0.005}^{2+}$ (a), $LiBaPO_4:Eu_{0.005}^{2+}$, $Pr_{0.005}^{3+}$, $Ca_2BO_3Cl:Ce_{0.002}^{3+}$, $Tb_{0.01}^{3+}$, $Yb_{0.01}^{3+}$ (b) at room temperature and the solar spectral and spectral response of c-Si (c).

Consequently, the heat energy leads to the thermalization of the charge carriers. In summary, the efficiency of Si solar cells is limited because of the energy loss resulting from thermalization of the charge carriers generated by the absorption of high-energy photons. But if UV-vis photons can be converted into NIR photons prior to absorption into Si solar cells (as shown in Fig. 3c), the charges thermalization of Si solar cells will be greatly decreased and the efficiency of Si solar cells will be improved.

Fig. 6a exhibits the PLE and PL spectra of $LiBaPO_4:Eu_{0.005}^{2+}$, which contains 4f–5d allowed transition of Eu^{2+} ions at 250–425 nm and a blue emission band at 480 nm.[21] It is worth noting that the Eu^{2+} single doped $LiBaPO_4$ has no emission band at NIR range. Fig. 6b gives the PLE and PL spectra of $LiBaPO_4:Eu_{0.005}^{2+}$, $Pr_{0.005}^{3+}$. Monitoring the emission at 1020 nm, the PLE spectrum contains a broad band and some sharp peaks. Comparing the PLE spectra of Eu^{2+} or Pr^{3+} singly doped in $LiBaPO_4$ phosphors (Fig. 6a and 2c), the intense broad band centered at 338 nm should be attributed to 4f–5d allowed transition of Eu^{2+} ions. The other peaks at 444 nm, 468 nm, 483 nm and 590 nm are due to f–f transitions of Pr^{3+} ions. Similar as Fig. 5a, the emission band peaked at 1020 nm is attributed to transition of $^1G_4 \rightarrow {}^3H_4$ of Pr^{3+}. The appearance of 4f $\rightarrow$ 5d transitions of Eu^{2+} ions in the PLE spectrum and the existence of the $^1G_2 \rightarrow {}^3H_4$ transitions of Pr^{3+} ion in the PL spectrum of $LiBaPO_4:Eu_{0.005}^{2+},Pr_{0.005}^{3+}$ indicate that the energy transfer from Eu^{2+} to Pr^{3+} occurs, as shown in Fig. 3. It demonstrates that $LiBaPO_4:Eu^{2+}$, Pr^{3+} can harvest UV-Vis photons of the incident solar spectral and significantly reduce the charges thermalization of Si solar cells by UV/vis-to-NIR spectral modification. At the same time, we compared our material with $Ca_2BO_3Cl:Ce_{0.002}^{3+}$, $Tb_{0.01}^{3+}$, $Yb_{0.01}^{3+}$, which was promising as useful light convert material for solar cell.[25] It is obviously that the emission intensity of our phosphor is about 5 times as intense as $Ca_2BO_3Cl:Ce_{0.002}^{3+}$, $Tb_{0.01}^{3+}$, $Yb_{0.01}^{3+}$ in NIR area. Therefore, it can be a promising light conversion material to increase the efficiency of Si solar cells.

4. Conclusions

Light conversion material $LiBaPO_4:Eu^{2+}$, Pr^{3+} was systematically investigated. We studied the spectral assignment of Pr^{3+} ions, and proved that the emissions at 599 nm and 617 nm are attributed to the $^1D_2 \rightarrow {}^3H_4$ and $^3P_0 \rightarrow {}^3H_6$ transfer according to the study of luminescence decay and spectra at low temperature. It is demonstrated that the energy transfer from Eu^{2+} to Pr^{3+} occurs in this matrix. Therefore, this phosphor has a wide excitation band in UV-vis region and emits intense NIR emitting around 1000 nm, which is matching well with the maximum spectral of Si solar cells. From the viewpoint of spectral modification, it may be a new light conversion material to match the solar spectrum and the spectral response of Si solar cells.

Acknowledgements

This work was financially supported by grants from National Nature Science Foundation of China (51602227), Scientific Foundation for Yong Teachers of Wuyi University (2016zk06), Doctor' Start-up Foundation of Wuyi University (2016BS10), Innovative Research Team in university of Guangdong (2015KCXTD027), Science Foundation for Yong Teachers of Wuyi University (2014td01) and the Science and Technology Projects of Guangdong Province (2015A090905010).

Notes and references

1 H. M. Zhang, H. R. Zhang, W. R. Liu, Y. L. Liu, Y. L. Liu, B. F. Lei, J. K. Deng, J. Y. Zhang, S. Y. Yan, H. K. Kuang and J. D. Zhang, *Ceram. Int.*, 2016, **42**, 16659–16665.
2 J. M. Wang, H. Lin, Q. M. Huang, G. C. Xiao, J. Xu, B. Wang, T. Hu and Y. S. Wang, *J. Mater. Chem. C*, 2017, **7**, 1789–1797.
3 L. T. Lin, X. M. Wu, T. Wang, D. J. Chen, C. Deng, J. X. Meng and L. W. Cao, *J. Alloys Compd.*, 2016, **673**, 411–419.
4 B. S. Richards, *Sol. Energy Mater. Sol. Cells*, 2006, **90**, 2329–2337.
5 Y. Y. Hao, Y. Wang, X. Y. Hu, X. X. Liu, E. Z. Liu, J. Fan, H. Miao and Q. Sun, *Ceram. Int.*, 2016, **42**, 9396–9401.
6 K. R. McIntosh, G. Lau, J. N. Cotsell, K. Hanton, D. L. Bätzner, F. Bettiol and B. S. Richards, *Prog. Photovoltaics*, 2009, **17**, 191–197.
7 M. J. Currie, J. K. Mapel, T. D. Heidel, S. Goffri and M. A. Baldo, *Science*, 2008, **321**, 226–228.
8 G. Seybold and G. Wagenblast, *Dyes Pigm.*, 1989, **11**, 303–317.
9 Z. H. Zou, L. Feng, C. Cao, J. C. Zhang and Y. H. Wang, *Sci. Rep.*, 2016, **6**, 24884.
10 S. Ye, B. Zhu, J. Chen, J. Luo and J. R. Qiu, *Appl. Phys. Lett.*, 2008, **92**, 141112–141114.
11 X. Hou, T. T. Xuan, H. C. Sun, X. H. Chen, H. L. Li and L. K. Pan, *Sol. Energy Mater. Sol. Cells*, 2016, **149**, 121–127.
12 X. P. Chen, X. Y. Huang and Q. Y. Zhang, *J. Appl. Phys.*, 2009, **106**, 063518–063521.
13 J. J. Eilers, D. Biner, J. T. van Wijngaarden, K. Kramer, H. U. Gudel and A. Meijerink, *Appl. Phys. Lett.*, 2010, **96**, 151106–151108.
14 B. M. V. D. Ende, L. Aarts and A. Meijerink, *Adv. Mater.*, 2009, **21**, 3073–3077.
15 Q. Y. Zhang, C. H. Yang, Z. H. Jiang and X. H. Ji, *Appl. Phys. Lett.*, 2007, **90**, 061914–061916.
16 C. de Mello Donega, A. Mejjerink and G. Blasse, Non-radiative relaxation processes of the Pr^{3+} ion in solids, *J. Phys. Chem. Solids*, 1994, **56**, 673–685.
17 S. Pinelli, S. Bigotta, A. Toncelli, M. Tonelli, E. Cavalli and E. Bovero, *Opt. Mater.*, 2004, **25**, 91–99.
18 S. Dang, J. B. Yu, X. F. Wang, L. N. Sun, R. P. Deng, J. Feng, W. Q. Fan and H. J. Zhang, *J. Lumin.*, 2011, **131**, 1857–1863.
19 S. Dang, L. N. Sun, S. Y. Song, H. J. Zhang, G. L. Zheng, Y. F. Bi, H. D. Guo, Z. Y. Guo and J. Feng, *Inorg. Chem. Commun.*, 2008, **11**, 531–534.
20 R. Y. Yang and K. T. Chen, *Mater. Res. Bull.*, 2014, **55**, 246–253.
21 S. Y. Zhang, Y. K. Nakai, T. J. Tsuboi, Y. L. Huang and H. J. Seo, *Chem. Mater.*, 2011, **23**, 1216–1224.
22 O. K. Moune, M. D. Faucher and N. Edelstein, *J. Lumin.*, 2002, **96**, 51–68.
23 M. T. Paques-Ledent, *J. Solid State Chem.*, 1978, **23**, 147–154.
24 J. M. Meijer, L. Aarts, B. M. van der Ende, T. J. H. Vlugt and A. Meijerink, *Phys. Rev. B*, 2010, **81**, 0354071–0354079.
25 Q. H. Zhang, J. Wang, G. G. Zhang and Q. Su, *J. Mater. Chem.*, 2009, **19**, 7088–7092.